A simplified approach to estimate seismic vulnerability and damage scenarios including site effects. Application to the Historical Centre of Horta, Azores, Portugal

N. Chieffo[a]*, T.M. Ferreira[b], R. Vicente[c], P.B. Lourenço[a], A. Formisano[d]

[a] ISISE, ARISE, Department of Civil Engineering, University of Minho, Portugal, Campus de Azurém, 4800-058 Guimarães, Portugal. Email: nicola.chieffo@civil.uminho.pt; pbl@uminho.pt

[b] School of Engineering, College of Arts, Technology and Environment (CATE), University of the West of England (UWE Bristol), United Kingdom. Email: Tiago.Ferreira@uwe.ac.uk

[c] RISCO, Department of Civil Engineering, University of Aveiro, Portugal.
Email: romvic@ua.pt

[d] Department of Structures for Engineering and Architecture, School of Polytechnic and Basic Sciences, University of Naples "Federico II", P.le V. Tecchio, 80125 Naples, Italy. Email: antoform@unina.it

corresponding author: nicola.chieffo@gmail.com; *nicola.chieffo@civil.uminho.pt*

A simplified approach to estimate seismic vulnerability and damage scenarios including site effects. Application to the Historical Centre of Horta, Azores, Portugal

The research attempts to provide a method for evaluating the susceptibility of heritage buildings and potential damage considering local site effects, using as case study an urban sector situated in Horta, Faial, Azores, Portugal. The physical vulnerability of the investigated structures was appraised using an index-based method devised for structural masonry aggregates to emphasize their likelihood to seismic damage. As a result, a damage scenario based on real accelerograms collected after the 1998 Azores seismic event was developed by using a reliable seismic intensity prediction equation. In addition, the soil amplification, which increases the extent of seismic damage to the examined structures, is assessed by varying the soil conditions using EN 1998-1 Code. Thus, this research emphasises the ground impact in forecasting the expected damage scenarios, enabling optimised risk mitigation strategies in urban settings.

Keywords: Site-Effects; Vulnerability Assessment; Unreinforced Masonry Aggregates; Damage Scenarios; Vulnerability Curves.

1. Introduction

Several seismic disasters have revealed the inadequate performance of the existing built cultural heritage, which has a wide range of construction types. This applies particularly to buildings constructed before seismic design requirements. The heterogeneity of urban areas and the scatter in socioeconomic development across the world, pose difficulties to the adoption of initiatives that limit disasters by mitigating seismic risk in urban areas (Salgado-Gálvez et al., 2016; Kassem et al., 2020). Seismic risk assessment aims at providing a descriptive and analytical estimation of potential losses as a result of earthquake activity in a specific territory, considering a specific timeframe. Vulnerability (V), Exposure (E) and Hazard (H), contribute to the definition of seismic risk, which may reach unacceptable values in many historic urban areas, e.g.

(Rapone et al., 2018). The reduction of seismic risk requires to investigate the seismic behaviour of structures when earthquakes occur (Vulnerability), the total amount of individuals and physical assets that could be endangered in the case of seismic activity (Exposure), as well as the severity and recurrence of the earthquakes (Hazard) (Chieffo et al., 2019; Basaglia et al., 2018; Calvi et al., 2006). The careful assessment of these factors is crucial for the definition of measures to ensure an acceptable risk level. Because the structural performance of buildings is influenced by many uncertainties, seismic risk is usually estimated probabilistically (Rapone et al., 2018). As a consequence, the expected impact is defined as unconditional, since it is not strongly related to a particular seismic activity, but arises as a result of the combined effect of all potential earthquakes originating from the *n*-seismogenic sources characterized by different intensity and probability of occurrence, as documented in (Chieffo et al., 2019; Basaglia et al., 2018; Calvi et al., 2006).

Recognizing the structures with the highest exposure in an urban context is complicated due to their structural variety and diversity. Moreover, the vulnerability of a building's stock to be affected by a strong earthquake is influenced by several factors, namely: (i) structural typology, (ii) material properties, and (iii) maintenance. Many studies (Brando et al., 2017; Lourenço & Roque, 2006; Lamego et al., 2017) have proven that existing buildings may be often considered ineffective against earthquakes. This may be due to inadequate construction practices and lack of local seismic culture.

A building inventory is essential for achieving data in terms of typological and structural characteristics. This inventory allows to adopt, systematically, a large-scale vulnerability procedure (Zuccaro & Cacace, 2015) to quantify the expected losses (Kircher et al., 2006; D’Ayala et al., 1997).

Empirical models are useful for estimating the seismic vulnerability on a broad scale by relying on a statistical analysis of historical earthquake data and observations of structural systems under seismic forces. These methods provide a realistic and efficient way for assessing the seismic susceptibility at territorial scale, as conducting numerical analyses on a city or country can be prohibitively expensive. Moreover, structural analysis requires extensive information about structural components, materials, and construction details, making such a tool less suitable for large-scale vulnerability studies. While significant progress has been made in analysing complex structures with the Finite Element Method (FEM) and the Discrete Element Method (DEM), these methods require a high level of knowledge and are computationally intense. For this reason, the use of FEM- and DEM-based vulnerability assessment has been mostly constrained to individual structures, in particular those with heritage value (Salachoris et al., 2023; Bianconi et al., 202; Milani & Clementi 2018; Clementi, 2021; Ferrante et al., 2021; Schiavoni et al., 2023). These methods enable a more accurate assessment, especially in case of complex geometries and heterogeneous materials. They also assist in identifying the most crucial structural sections and in guiding the selection of appropriate retrofitting solutions.

The development of a seismic loss model in a specific location is crucial, not only for the financial implications of future disasters, but also for relevant mitigation strategies related to different risk scenarios (Vicente et al., 2011b; Maio et al., 2016; Ferreira et al., 2013a). In addition, a seismic loss model allows the selection of effective implementation strategies for dealing with emergency planning, with tailored measures to protect the population and the historical built heritage (Bramerini & Lucantoni, 2000).

Nowadays, a significant issue in earthquake risk assessment is the quantification of geotechnical site effects, since it enables a more realistic estimation of potential damage. Soil layers play a critical role in the behaviour of seismic waves at the lithosphere surface. Unfavourable geological settings can lead to significant amplification of the motion propagation surface, resulting in more significant accelerations transmitted to the foundation of the buildings. The magnitude of these accelerations tend to be greater in soils with worse geotechnical characteristics (Dolce et al., 2006; Brando et al., 2020; Azizi-Bondarabadi et al., 2016). Water also contributes to seismic wave amplification. Seismic waves passing saturated soils cause an increase in water pressure, reducing effective stress and stiffness, thereby intensifying ground motion and potentially leading to increased seismic amplification and structure damage. Liquefaction is another potential phenomenon in the presence of saturated soils. In these cases, saturated soils behave like a liquid, leading to severe damage to structures and infrastructure. Therefore, future studies should consider the role of water effects to develop a more comprehensive understanding of a region's seismic hazard.

The identification of local site effects can be achieved by treating the soil model as a 1D or 2D half-space. The primary distinction between these models is that in a 1D analysis, only the depth of the half-space is addressed, ignoring the transverse boundary conditions. The comprehensive 2D examination, on the other side must include a considerable volume of soil in the longitudinal and vertical planes. Local site effects can also be investigated (Afak, 2001): (i) in the spectral domain; (ii) in the bandwidth domain. In the first case, the local amplification factor is estimated at the bedrock substrate accounting for the soil amplification at the ground surface. In the second case, the amplification factor can be calculated using either the Fourier amplitude spectra or the response spectrum, which is a frequency domain technique. Nevertheless, simplified approaches for estimating site effects and their implications on seismic risk have been developed. The methodologies proposed by (Giovinazzi, 2009b) and (Chieffo &

Formisano, 2019b) allow the evaluation of the increase of the expected earthquake intensity (Grünthal, 1998) based on a particular soil condition.

The current research aims to evaluate local amplification conditions and provide a parametric-based approach to estimate damage scenarios for the historical centre of Horta in Portugal, using a time domain model. This work builds on previous research presented by (Ferreira et al., 2017b), where the authors conducted a vulnerability analysis of this study area. However, the potential impact of site-effects was neglected, which is a novel contribution of the present paper. Recognizing that external factors such as geology and topography have a considerable impact on the structural integrity and safety of a building, the proposed research can identify which structures require the most urgent attention and intervention. Overall, the main contribution of this paper is the proposal of an easy-to-use procedure to evaluate site effects in large-scale vulnerability analysis, which can be used to provide insight into the impact of the surrounding environment on existing buildings. This knowledge allows to prioritize intervention efforts aiming at improving the safety and structural integrity of buildings identified as seismically vulnerable.

2. Seismic vulnerability assessment of the historical centre of Horta

2.1. Identification of the case study area

Horta is a Portuguese municipality of around 15 000 individuals residing in Faial Island, Azores Island (Ferreira et al., 2017b), see Figure 1. The historical nucleus of the city develops along its main route, also known as Avenida Marginal or Avenida D. Infante Henriques, and is intersected by smaller streets and courtyards. A secondary nucleus was formed in the Porto Pim region, which later grew to an urban continuous agglomeration formed along the coast.

Figure 1. Geographical localization of Horta.

2.2. Seismicity of the study area

The convergence of the African, European, and North American plates characterises the Azores Islands. The plate's boundaries are prone to earthquakes since they absorb stresses induced by plate displacements and dissipate energy during major earthquakes. As a consequence, the 1941 M_w=8.1 Gloria Fault earthquake and the 1975 North Sea earthquake, both related to strike-slip faults rupture, were two of the largest seismic events documented near the Azores. Afterwards, the 1998 Faial earthquake struck the Azores Islands of Portugal at 05:19 am local time. Although being located offshore in the Atlantic Ocean, the shallow mainshock with M_w=6.2 produced significant damage (Figure 2) (Zonno et al., 2008).

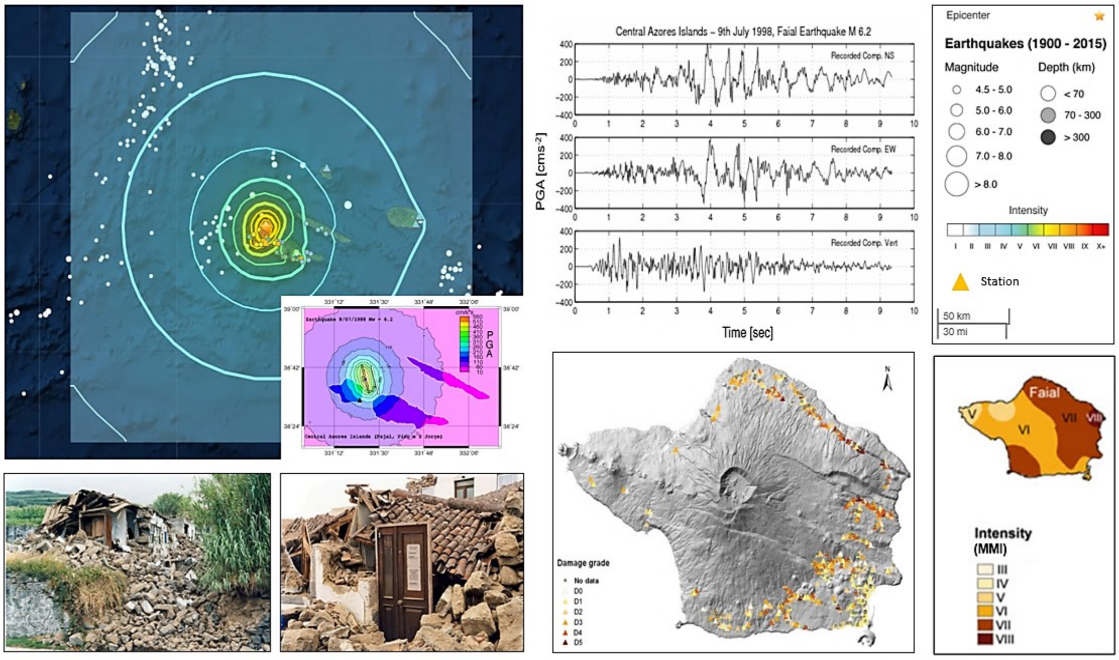

Figure 2. Epicentre location of the 1998 Azores earthquake and damage distribution on Faial Island (Zonno et al., 2008).

The earthquake severely damaged or destroyed approximately 35% of all buildings on Faial Island and 10% of structures on neighbouring Pico Island, bringing the total number of structures affected to 3909.

Generally, the archipelago presents a consistent use of irregular masonry for the walls, together with timber floors and roofs. Earthquake damage included complete collapse of the masonry walls and extensive cracks localised in the perimetral walls. (Ferreira et al., 2017b) provides the building damage according to the EMS-98 scale (Grünthal, 1998). This allows geographical investigations, such as determining the distribution of buildings associated with a particular level of damage in a specific area. The earthquake seriously affected numerous masonry churches, with the collapse of loadbearing walls and widespread damage. Figure 3 shows archival data related to the damage caused by the 1998 Azores earthquake.

(a) Ribeirinha, Faial Island (b) Ribeirinha, Faial Island (c) Ribeirinha, Faial Island

(d) Pedro Miguel, Faial Island (e) Madalena, Pico Island (f) Castelo Branco, Faial Island

Figure 3. Examples of damage observed in different locations after the 1998 Azores earthquake.

2.3. Building inventory of the study area

The historic centre in the city of Horta is structurally and typologically rather similar. The urban sector considered here consists of 313 buildings in aggregate condition (i.e. connected to other buildings, and not isolated). The buildings were classified into four distinct groups of common structural characteristics: Group I consisted of detailed unreinforced masonry aggregates (URM), for which adequate data is available; Group II includes non-detailed URM buildings, for which scarce information is available; Group III includes reinforced concrete structures (RC), and Group IV includes non-accessible structures of unknown type, here referred to as special structures.

Group I, of 50 buildings (16% of the sample), allows a review of detailed drawings and observed damage, providing the necessary input parameters for the seismic vulnerability. Because only an external visual inspection was possible for

Group II, these 142 structures (45%) were categorized as not-detailed. Group III consists of 93 RC buildings (30%) and Group IV consists of 28 structures (9%). The present study is based on structural masonry aggregates; therefore, Groups III and IV were excluded from the vulnerability analysis.

The vulnerability methodology described in the following section was adopted for detailed and non-detailed URM groups (Ferreira et al., 2017b). From a structural point of view, the most common masonry stone walls are composed of basalt, trachyte, and volcanic tuff. The walls are 0.60 m thick on average, with clay and lime plaster on both sides. Most analysed masonry buildings lack ring beams or steel tie-rods at the floors or roof level. The floors are typically composed of timber elements, whereas the roofs are usually made of double-pitch timber rafters (with and without truss structure) with clay tiles (Costa, 2002).

The elevation of the masonry buildings is variable, with a minimum of one story and up to three stories. The inter-story height at the ground level ranges from 3.00 m to 4.00 m, and from 3.00 m to 3.50 m on the upper floors. The foundation system is shallow wall footings, built by placing the masonry walls directly on the ground at a depth of roughly 1.50 m. To characterise the investigated masonry buildings (Group I and Group 2), the following abbreviations were used: URM-L (one-story, unreinforced masonry low-rise – 14%), URM-M (two stories, unreinforced masonry medium-rise – 63%), and URM-H (three stories, unreinforced masonry high-rise – 23%). The building data was managed in the GIS environment, see Figure 4 (a) and (b), before being statistically elaborated to provide information concerning the examined building groups. Figures 4 (c) and (d) outline the collected data in terms of number of buildings.

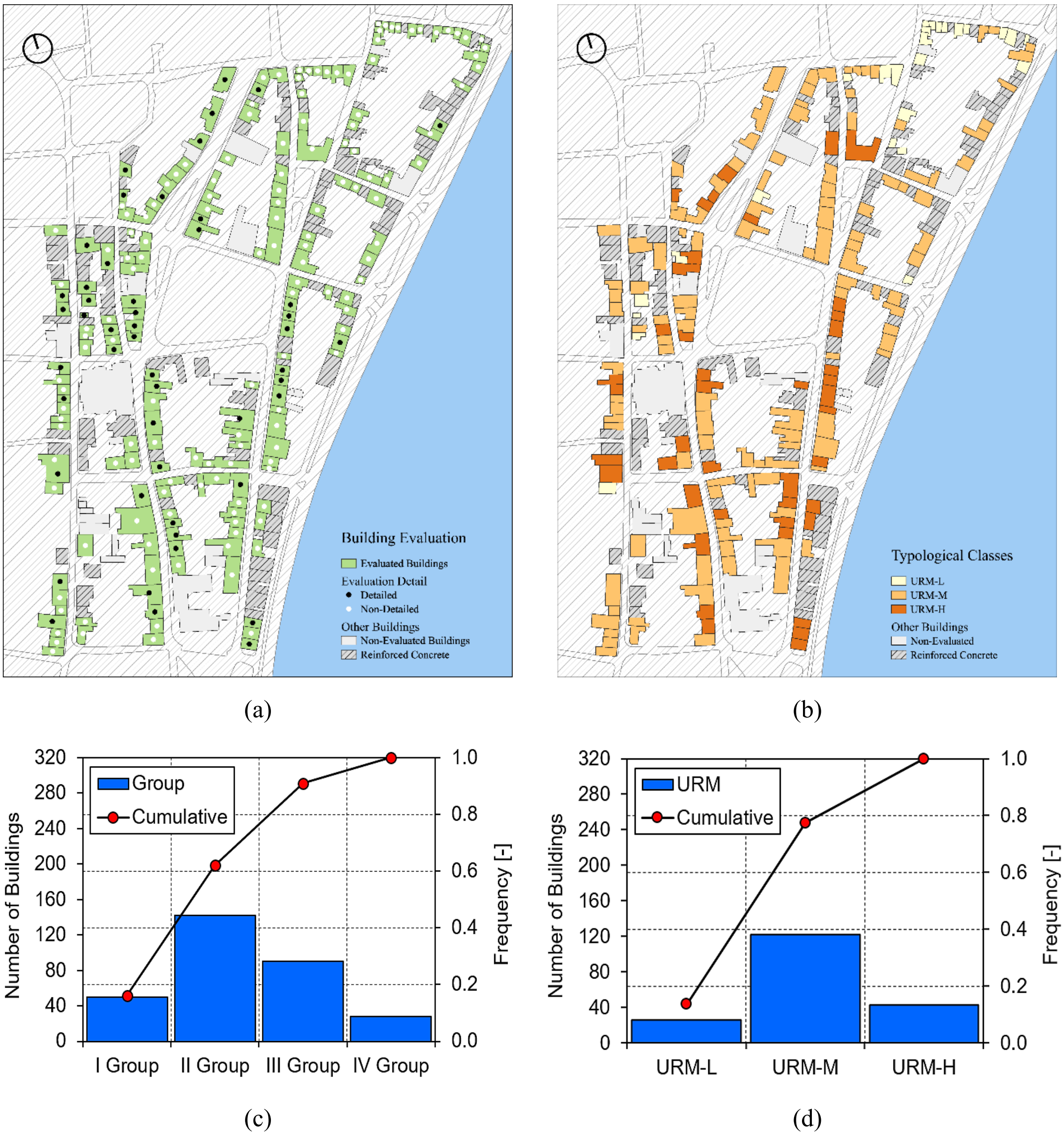

Figure 4. Preliminary characteristics of the surveyed buildings: evaluation details (a); typological classification (b); inventory of the building stock (c) (Group I (detailed URM), Group II (non-detailed URM), Group III (RC structures), Group IV (special buildings); classification of URMs classes based on the number of stories (d).

2.4. Post-earthquake damage data

An initial screening of the observed damage was carried out using post-earthquake data from the 1998 Azores seismic event, which struck the central part of Portugal's Azores archipelago. The event resulted in 8 dead, 150 injured and 1500 homeless people (Ferreira et al., 2017b; Zonno et al., 2008). The earthquake had a Modified Mercalli

Intensity scale, MMI, that reached VII, as reported in Figure 5, and the damage was collected in a detailed catalogue. This damage catalogue incorporates the typical failure mechanisms of the masonry traditional houses (Zonno et al., 2008). It is worth mentioning that the damage was assessed originally using the MMI intensity scale, whereas the EMS-98 intensity scale proposed in (Grünthal, 1998) was adopted and compared to the MMI one in (Ferreira et al., 2017b).

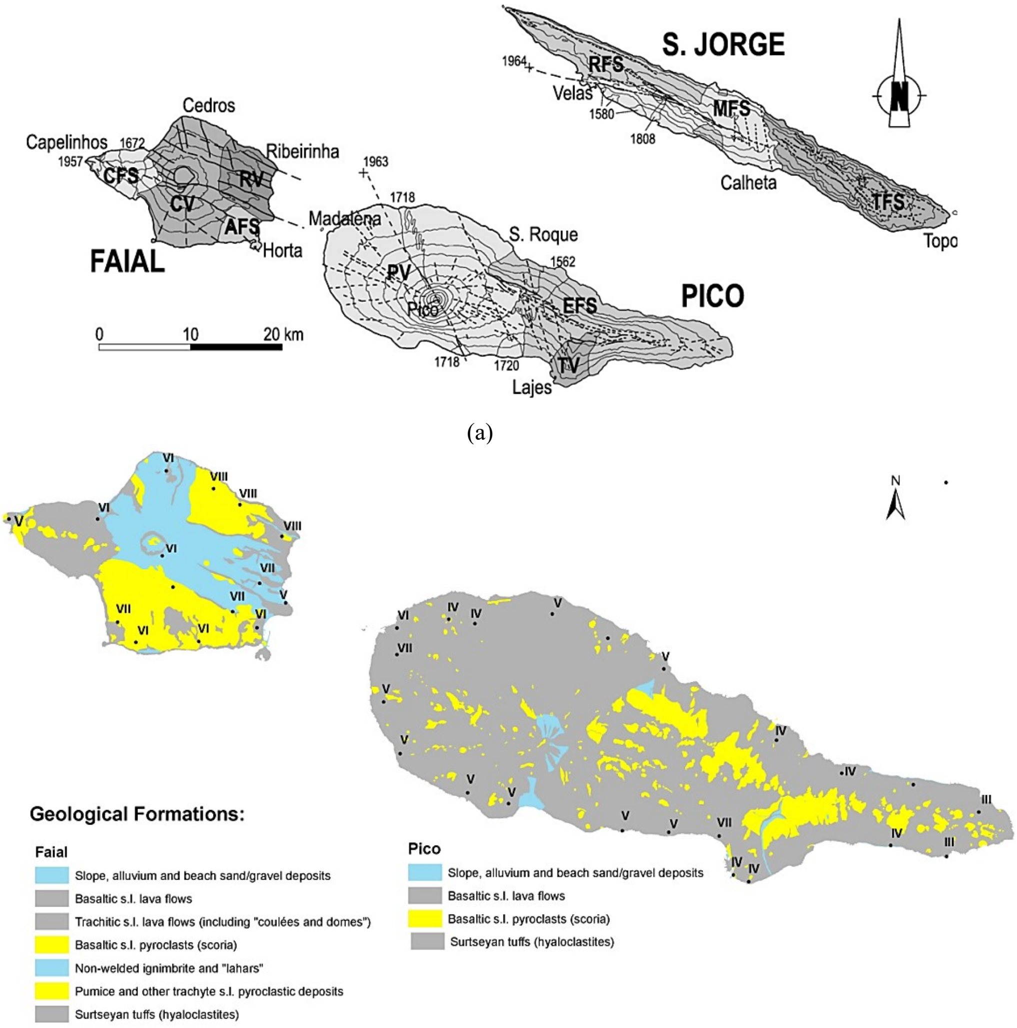

(a)

(b)

Figure 5. The geomorphological map of the Faial and Pico islands (a), as well as the observed intensities indicated by the Modified Mercalli Intensity scale (b) (Zonno et al., 2008).

Table 1 shows the distribution of the damage, using the EMS-98 scale, associated with the building stock in 11 districts, i.e. the smallest unit of local government (Costa, 2002; Ferreira et al., 2017b; Zonno et al., 2008). Different studies, e.g. (Rosti et al., 2021; Rota et al., 2008) and (Biglari et al., 2021), have emphasised the importance of damage assessment in high seismic risk urban contexts. These correlate structural characteristics of buildings with the amount of damage and recommend streamlined empirical models for evaluating building usability based on macroseismic intensity and construction parameters (Mosoarca et al., 2020; Lagomarsino et al., 2021; Biglari & Formisano, 2021; Di Ludovico et al., 2017).

Table 1. Distribution of the building damage detected after the 1998 Azores earthquake.

ID	Intensity	District	Observed damage, D_{Ki}					
			D0	D1	D2	D3	D4	D5
1	VII	Angústias	-	7	-	-	-	-
2	VII	Castelo Branco	-	1	3	1	-	-
3	VI	Cedros	-	3	3	-	-	-
4	V	Conceiãao	1	8	2	1	-	-
5	VI	Feteira	-	3	1	1	-	-
6	VII	Flamengos	-	-	2	1	2	-
7	VII	Matriz	1	13	2	-	-	-
8	VII	Pedro Miguel	-	-	-	2	2	1
9	VII	Praia do Almoxarife	-	7	5	4	-	-
10	VIII	Riberinha	-	-	-	3	2	2
11	VII	Salão	-	2	1	1	1	-
		Total	2	44	19	14	7	3

Damage Probability Matrices, DPM, (see Figure 6) were implemented to quantify the observed damage in the 1998 Azores seismic event using the binomial distribution function based on the weighted average of damage, μ_D, as:

$$\begin{cases} p_k = \dfrac{5!}{k!(5-k)!} \cdot \left(\dfrac{\mu_D}{5}\right)^k \cdot \left(1 - \dfrac{\mu_D}{5}\right)^{5-k} \\ \mu_D = \sum_{k=1}^{5} p_k \cdot k \end{cases} \tag{1}$$

where k is a quantitative parameter associated with the damage level, ranging from 0 to 5 on the EMS-98 scale, and p_k represents the evaluated relative frequencies (Chieffo & Formisano, 2019b).

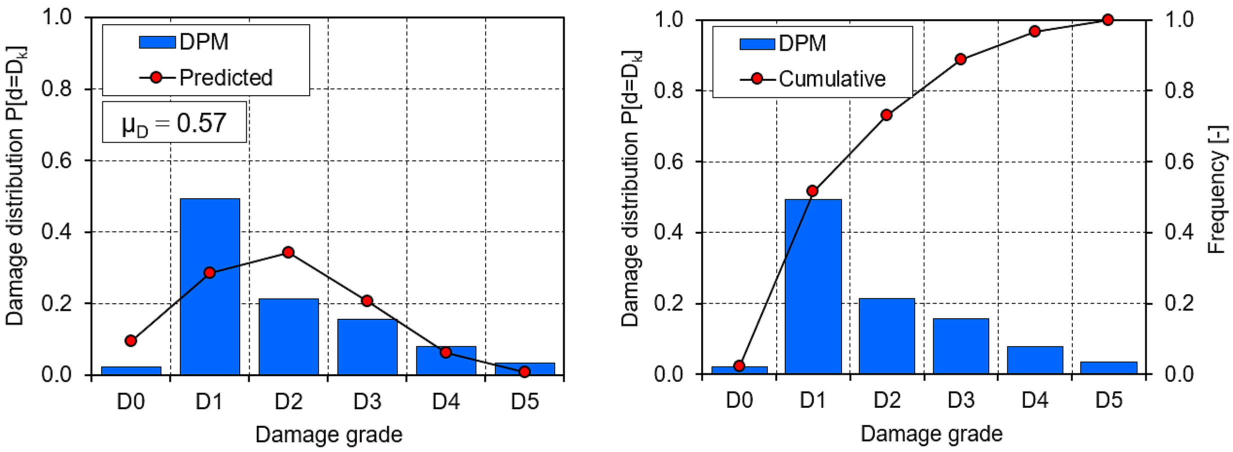

(a) (b)

Figure 6. Damage: Damage Probability Matrices (DPMs) observation, prediction by binomial distribution and weighted average of damage (a); cumulative distribution (b).

The expected frequencies for the examined post-earthquake damage data are shown in Figure 6 (a). The observed cumulative damage is given in Figure 6 (b): 2% of the investigated structures have no damage (D0); 49% have slight damage (D1); 22% have moderate damage (D2); 16% have severe damage (D3); 8% are near collapse (D4); and 3% have collapsed (D5).

2.5. Vulnerability procedure

The vulnerability of Horta's historical centre was assessed using the vulnerability index methodology, which has been gaining growing preponderance in recent years to identify the seismic vulnerability of masonry buildings in urban settings (Ferreira et al., 2013b, 2017b; Vicente et al., 2011b). This vulnerability index considers a variety of factors that contribute to a building's seismic susceptibility, such as structural characteristics, age and potential hazard. The approach gives a quantitative assessment of a building's vulnerability by assigning a numerical value to different weighted parameters (Ferreira et al., 2013b, 2017b; Vicente et al., 2011b). The process can be used for a large number of buildings in an urban area, allowing for the identification of high-risk structures that require attention. The results help to decide actions regarding building retrofitting, demolition, or other interventions aimed at increasing urban safety and resilience.

In this context, a scoring index-based method developed originally by (Vicente et al., 2014; Ferreira et al., 2014; Ferreira et al., 2017a) (see Table 2) was used to evaluate the susceptibility of buildings through predefined categories that take into account the specificities and structural deficiencies of a generic structural system influenced by expert judgement regarding weights and scores. The suggested vulnerability form is composed of fourteen fundamental factors that are subdivided into four major groups to assess the essential qualities of the building's response (Ferreira et al., 2013b, 2017b; Vicente et al., 2011b):

- First group: Structural building system. This group has six parameters and outlines the general building-resistant system, the type and quality of walls, texture, and masonry configuration, as well as the quality of wall-to-wall connectivity. Furthermore, parameters P1 and P4 generally assess the shear strength capacity and potential collapse mechanisms, while the other two parameters, P5 and P6, examine the height and soil conditions.

- Second group: Irregularities and interactions. This group has three parameters and explores the different behaviour of a building compound during a seismic event by focusing on its relative position and interaction with other structural parts. This group also differentiates the morphology of the building by irregularities in plan and height, as well as the percentage of openings in the façade. The higher the percentage difference in the opening between two adjacent façades, the worse the horizontal load distribution between them.
- Third group: Floor slabs and roofs. This group has two parameters and assesses horizontal structural systems, namely the type of timber floor connection and the impulsive character of pitched roofing systems.
- Fourth group: Conservation status and other elements. This group has two parameters and examines the building's structural deficiencies and condition.

Table 2. Adopted vulnerability form for the case study sample (Ferreira et al., 2014).

Parameters by group	Class, C_{vi}				Weight, p_i	Relative weight over I_V^*
	A	B	C	D		
Group 1. Structural building system						
P1 Type of resisting system	0	5	20	50	0.75	50/100
P2 Quality of the resisting system	0	5	20	50	1.00	
P3 Conventional strength	0	5	20	50	1.50	
P4 Maximum distance between walls	0	5	20	50	0.50	
P5 Number of floors	0	5	20	50	1.50	
P6 Location and soil conditions	0	5	20	50	0.75	
Group 2. Irregularities and interactions						
P7 Aggregate position and interaction	0	5	20	50	1.50	20/100
P8 Plan configuration	0	5	20	50	0.75	
P9 Height regularity	0	5	20	50	0.75	
P10 Wall façade openings and alignments	0	5	20	50	0.50	
Group 3. Floor slabs and roofs						
P11 Horizontal diaphragms	0	5	20	50	1.00	18/100
P12 Roofing system	0	5	20	50	1.00	
Group 4. Conservation status and other elements						
P13 Fragility and conservation status	0	5	20	50	1.00	12/100
P14 Non-structural elements	0	5	20	50	0.50	

The corresponding values of the associated vulnerability class, C_{vi}, are categorised into four vulnerability classes (A, B, C, and D, from best, A, to worst, D), each with a score between 0 and 50. Each parameter estimates a specific attribute associated with a building's capacity and therefore is assigned a weight, p_i. The weights ranges from 0.50 for the least critical factors to 1.50 for the most important factors. More information on how the scores and classes were attributed may be found in (Ferreira et al., 2014).

The vulnerability index, I^*_V, is calculated as the weighted combination of the class score chosen for each of the 14 factors listed in Table 2 multiplied by the corresponding weight. As a result, the index I^*_V is derived as follows:

$$I^*_V = \sum_{i=1}^{14} C_{vi} \cdot p_i \tag{2}$$

where, C_{vi}, is the specific score associated with each parameter, and p_i is the assigned weight.

The introduced index resulting from Eq. (2) varies between 0 to 650 and has been normalised between 0 and 100, assuming then the I_v designation, subsequently used in this paper. Based on these assumptions, the spatial vulnerability index I_v distribution for the investigated urban area is depicted in Figure 7.

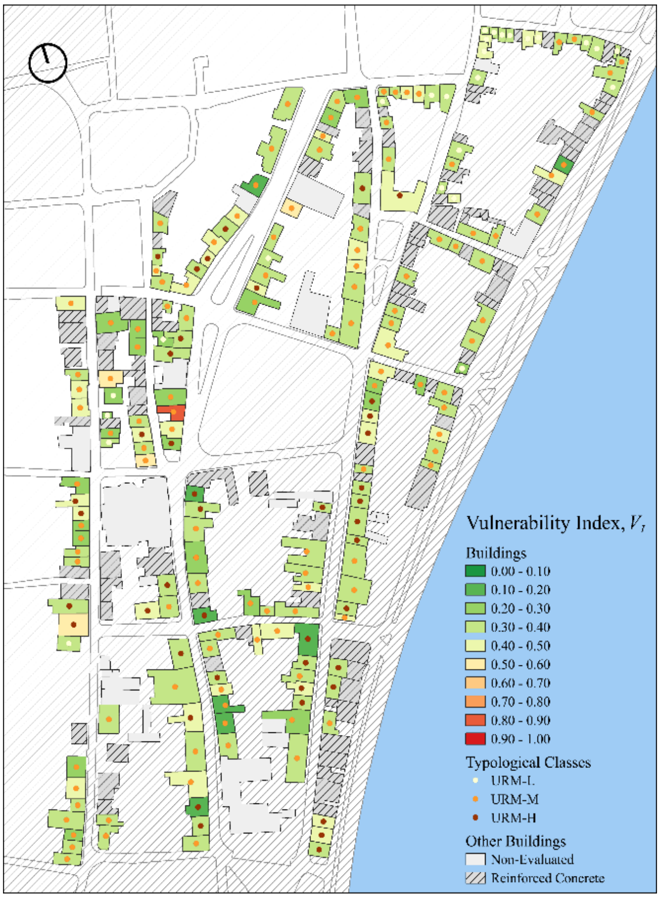

Figure 7. Vulnerability index distribution for the Municipality of Horta.

In addition, the results obtained were statistically processed (see Figure 8), showing the predicted vulnerability distribution and corresponding frequencies. In particular, in Figure 8 (a), the index values, I_v, derived from the above-mentioned assessment approach more common range between 33 and 38, accounting for 59% of the buildings sample. The maximum values I_v values occur in the interval between 77 and 82 (only 1% of the cases). Furthermore, the cumulative distribution is shown in Figure 8 (b).

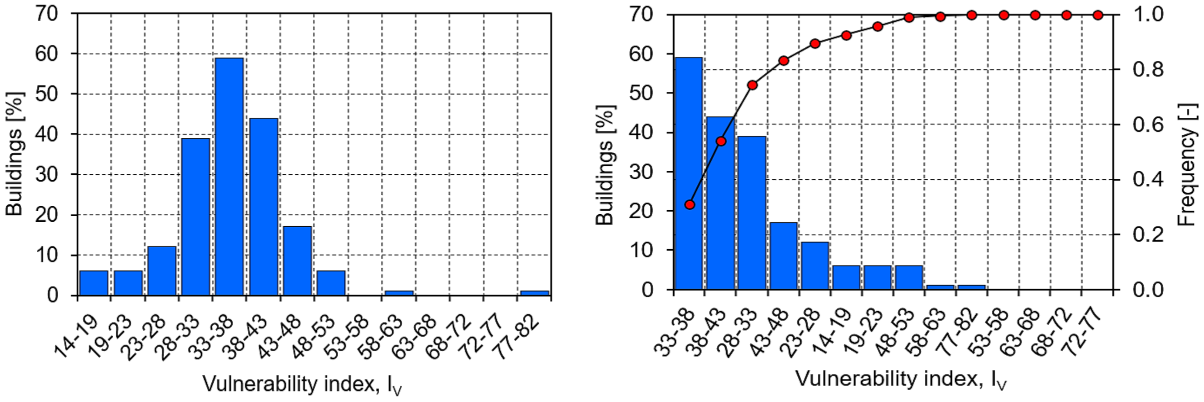

(a) (b)

Figure 8. Vulnerability index distribution (a) and (b) cumulative function for the inspected buildings.

Vulnerability curves (Lagomarsino et al., 2021) have been developed to quantify the expected damage ($0 < \mu_D < 5$) according to (Grünthal, 1998). The curves have been computed as:

$$\mu_D = 2.5 + 3 \cdot \tanh \cdot \left(\frac{I + 6.25 \cdot V - 12.7}{Q} \right) \cdot f(V, I)$$
$$f(V, I) = \begin{cases} e^{\frac{V}{2} \cdot (I-7)}, & if\ I \le 7 \\ 1, & if\ I > 7 \end{cases} \tag{3}$$

where I represents the intensity level, V identifies the vulnerability index (see Eq. (4)) and Q is the ductility (ranging from 1 to 4 depending on the building typology. A value equal to 3 was assumed here). It is noted that the ductility factor Q should be calibrated appropriately based on the peculiarities of the stock of buildings investigated. Moreover, the term $f(V, I)$ is a function that, as reported by (Zonno et al., 2008), correlates the estimated index to the expected macroseismic intensity I to take into account the numerical trend of the vulnerability curves for lower impact grades, i.e. I = V and VI. Ultimately, for the quantification of the aforementioned damage grade μ_D, the vulnerability index I_v is associated with the vulnerability index V as:

$$V = 0.592 + 0.0057 \cdot I_V \qquad (4)$$

The mean damage curves provided in Figure 9 estimate the amount of expected vulnerability range for the examined buildings considering the statistical range, $I_v \pm \sigma$; $I_v \pm 2\sigma$ (see Figures 9 (a) to (c)), as described in (Ferreira et al., 2017a; Mosoarca et al., 2020). Here, σ is the standard deviation of the mean damage grade. Moreover, the corresponding observed damage depicted in Section 2.4 has been related to the mean damage curves in Figures 9 (d) to (f).

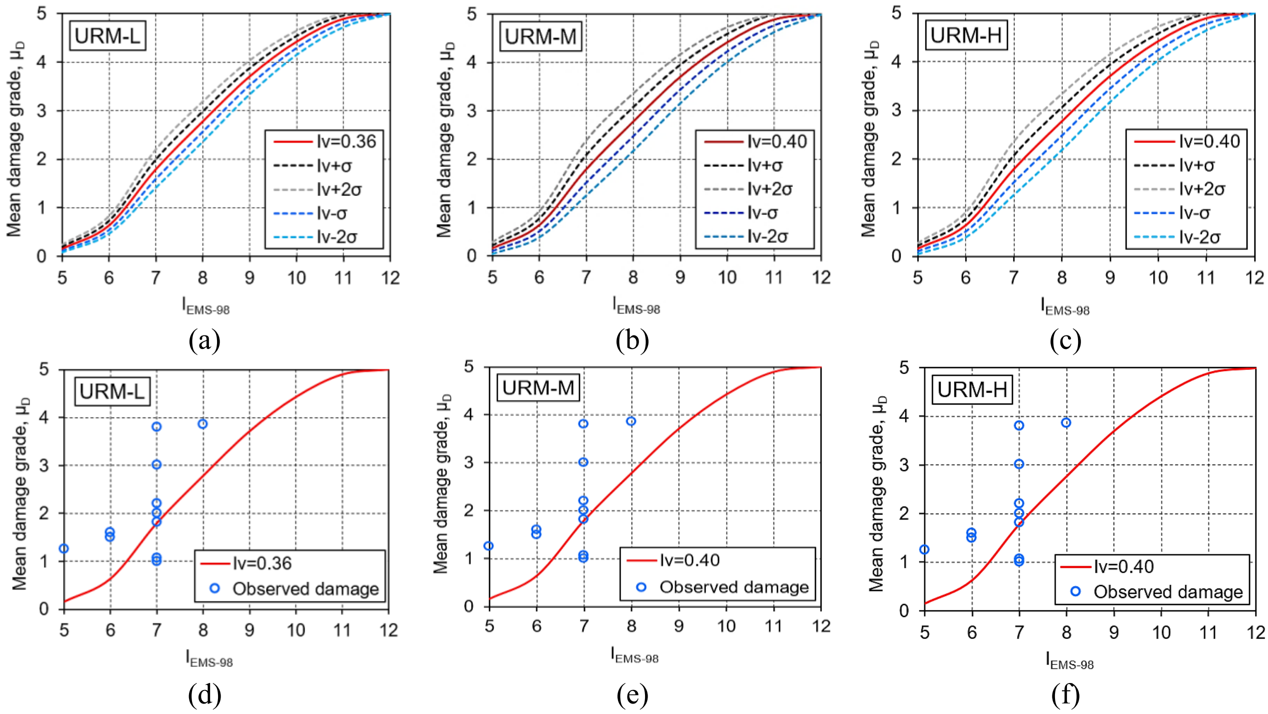

Figure 9. Mean damage curves for the examined building typologies (a-c), and the related damage observed after the 1998 earthquake (d-f).

The results indicate that the vulnerability distribution predicts a consistent average I_v value of 0.36 and 0.40 for all typological classes investigated (URM-L, URM-M and URM-H). The amplitude of the statistical distribution range is larger with increasing number of floors, when compared to single story buildings. These results support the theory that higher-rise buildings suffer more damage than mid-rise ones, as the vulnerability standard deviation (σ_i) associated with each building class are σ_{URM-L}=0.06, σ_{URM-M}=0.085, and σ_{URM-H}=0.083.

3. Damage scenario

For management and mitigation purposes, risk is usually defined as the economic, societal and environmental consequences of a catastrophic event that may occur in a given period. A prediction of potential damage consequences caused by natural events is a useful tool for quantifying expected losses in a specific area and implementing mitigation measures. Mainly, the susceptibility to damage depends on the quantification of the resources exposed to risk (Chieffo & Formisano, 2019c).

The severity of the seismic damage is analysed here using a parametric analysis. It is evident that during an earthquake, the buildings will be subjected to damage that is proportional to the severity of the seismic motion. The energy released during a seismic event is characterized by the propagation of seismic waves, which depart at different velocities in all directions with approximately spherical wavefronts. There is an attenuation of the energy of seismic waves from the epicentre to the different sites where the earthquake effects are felt, since the amplitude of the volume waves decreases proportionally to the seismogenic site-source distance, D, while for surface waves the amplitude decreases by about $1/\sqrt{(D)}$ (Chieffo & Formisano, 2019a). The prediction of the seismicity for a given site can be assessed by adopting an appropriate seismic attenuation law. Attenuation models are empirical formulations calibrated from statistical data (instrumental or macroseismic) of observed earthquakes. Generally, these laws are based on simplified models to represent seismic propagation (Atkinson & Kaka, 2007; Toro et al., 1997).

In practice, an empirical relationship may be established between simple factors (energy released at the source through the magnitude (M_w), distance (D) or depth (h) between epicentre and site) and a set of coefficients that best reproduce the set of instrumental or macroseismic observations (Atkinson & Kaka, 2007; Toro et al., 1997). Multiple formulations have been developed, validated and proposed according to the Global Earthquake Model Foundation catalogue (Bozorgnia et al., 2010). Attenuation models were generated in terms of spectral accelerations and displacements (S_a and S_d), peak ground accelerations (PGA) or seismic intensity (MMI), deduced from instrumental recordings of occurred past earthquakes (Bozorgnia et al., 2010). Here, the severity of seismic effects has been analysed predictively using the conversion model proposed by (Masi et al., 2020), which is given by the following expression:

$$I_{\text{EMS-98}} = 0.89 \cdot \ln(\text{PGA}) + 8.05 \tag{5}$$

This equation associates the intensity using the EMS-98 scale, $I_{\text{EMS-98}}$, to the natural logarithm of PGA, expressed in g. It is noted that, for seismic intensities lower than grade VI, the direct effect on the building stock is generally negligible, while for $I_{\text{EMS-98}} > \text{VI}$, the damage caused to buildings becomes predominant, offering stable results. Based on this, the accelerograms recorded on Central Azores Island for the 1998 Azores seismic event have been considered (Zonno et al., 2008). In particular, considering the three main directions, i.e., NS (North-South), EW (East-West), and Vertical direction, the examined damage scenario contemplates the maximum contribution in terms of the observed PGAs.

The observed NS and EW ground motion components offer the largest contribution in terms of PGA amplitude, which corresponds to a maximum PGA of 4.0 ms^{-2}. Thus, the correlation obtained between PGA ($g \approx 10$ ms^{-2}) and macroseismic intensity, $I_{\text{EMS-98}}$, is summarised in Table 3.

Table 3. Correlation between ground acceleration, PGA, and macroseismic intensities, $I_{\text{EMS-98}}$.

Direction	PGA (ms^{-2})	PGA (g)	$I_{\text{EMS-98}}$

NS (EW)	4.0	0.4	VII

The conversion formula forecasts a macroseismic intensity of XII, which corresponds to what occurred in the study area ($I_{\text{EMS-98}}$=VI, see Figure 5). Then, the correlation between the average damage grade, μ_D, and the damage thresholds, D_K, is given in Figure 10 (Whitman et al., 1974). From the results, the average damage grade, μ_D, for the URM-L class is equal to 0.20 with 100% of the investigated buildings in damage D1 (Slight damage). Instead, for the URM-M class, μ_D is equal to 0.39, which is associated with 8% of buildings having a damage level equal to D1, whereas 90% of the buildings suffer damage D2 (Moderate damage) and only 2% damage D3 (Significant damage). Finally, URM-H is associated with a μ_D equal to 0.38, corresponding to 12% and 88% of the buildings suffering damage D1 and D2, respectively.

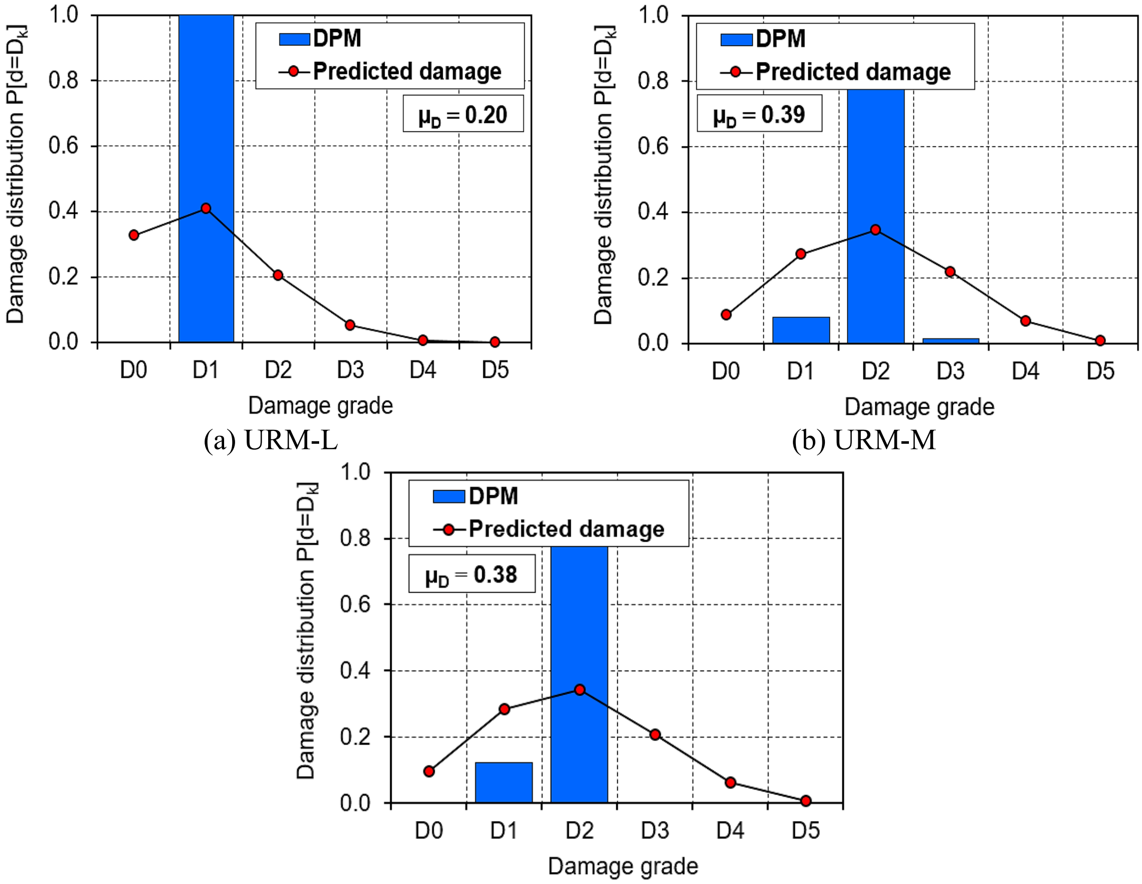

Figure 10. Damage distributions for the analysed buildings stock.

4. Site effects

4.1. Evaluation of the amplification factor

The hazard analysis primarily seeks to quantify the expected seismic input in a specified place concerning a specific intensity measurement, IM, correlated with macroseismic intensity for territorial-scale assessment, presumably including local amplification effects (Lanzo et al., 2011). Site conditions, combined with variable topography, can strongly impact the amplitude, frequency, and duration of a strong motion and, as a consequence, will affect the buildings' response, amplifying the expected damage (Boore & Joyner, 1997). Ground motion models are often expressed in spectral domain and frequency domain. Specifically, when evaluating the spectral domain, the most commonly used variables to define the earthquake's characteristics are the peak ground acceleration, velocity or displacement, and duration. The seismic motion parameters in the frequency domain are determined by the Fourier spectrum or the response spectrum (Chieffo & Formisano, 2020). To ensure appropriate analysis of local phenomena, the dynamic amplification is assessed using the elastic design spectrum according to the EN 1998-1 Code (Eurocode, 2004), as reported in Figure 11.

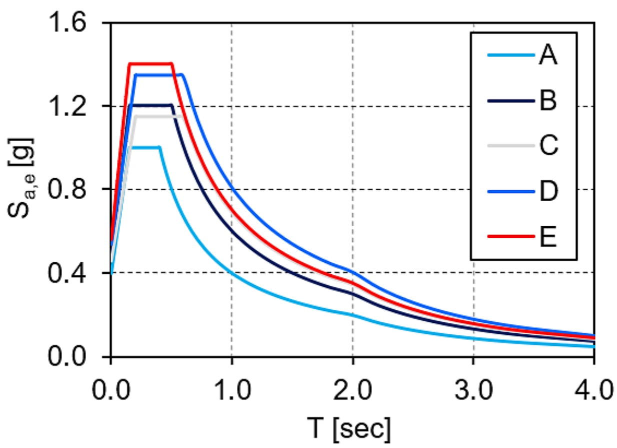

Figure 11. EN 1998-1 Code design response spectrums.

The site amplification factor, f_{ag}, is the ratio between the maximum acceleration S_{ae} of the design spectrum, computed for a generalised type of soil, K, $S_{ae}(T)_K$, and the corresponding response spectrum for rigid soils, given in (Giovinazzi, 2009b) as:

$$f_{ag} = \frac{S_{ae}(T)_K}{S_{ae}(T)_R} \tag{6}$$

Then, the seismic intensity increase, ΔI, is calculated using the following relationship:

$$\Delta I = \frac{\ln(f_{ag})}{\ln C_2} \tag{7}$$

Here, according to (Giovinazzi, 2009b), the coefficient C_2 is 1.82 when evaluating a Type I design spectrum for a moderate magnitude earthquake ($M_w > 5$) at a close distance. Furthermore, the influence of the behaviour factor (or response modification factor) on the seismic vulnerability can be defined as ΔV_I. This directly impacts the global physical susceptibility of the buildings, (Giovinazzi, 2009b), providing a seismic vulnerability increment given by:

$$\Delta V_I = \frac{\Delta I}{6.25} \tag{8}$$

The approach presented in (Giovinazzi, 2009b) to determining site effects is widely used in earthquake engineering. This method has advantages and disadvantages, which should be considered before determining whether to utilise it in a particular study. The simplicity of the approach is one of its key advantages. The approach requires only a few input parameters, making it very low computationally intensive. The technique has been proven in multiple studies also to produce good estimates of site reaction, making it a helpful tool for site-specific seismic hazard assessment. Still, for soil layers, the method requires a homogenous half-space model, which may not be appropriate in all circumstances. This is a serious disadvantage for sites with complicated soil stratigraphy, because the approach may not capture the impacts of 3D soil heterogeneities accurately. Furthermore, when used in sites with significant impedance differences between layers, the approach may also provide inaccurate results. Additionally, the approach may be inaccurate in locations where seismic waves interact with topography or near-surface geologic structures.

The studies presented by (Bindi et al., 2021; Raptakis et al., 2018; Spadafora & Alberico, 2017) introduce new developments and insights into the evaluation of urban site effects, namely regarding novel methodologies for assessing seismic hazards and mitigating risk. These studies highlight the necessity to consider site effects when assessing seismic susceptibility and provide a better knowledge of the influence of local site characteristics on ground motion amplification by researching various metropolitan locations. Overall, these works contribute significantly to the subject of earthquake engineering and provide useful information to researchers and those interested in seismic hazard assessment and risk management.

4.2. The site effect on the expected vulnerability of building typologies

The seismic vulnerability was assessed by taking into account the above-identified factors using a parametric analysis for various soil characteristics according to the design spectra (Type I) derived from the EN 1998-1 Code (Eurocode, 2004). The Azores' island's sediments are composed primarily of recent volcanic minerals that originated in the humid and moderate Atlantic environment. These lithologies are rare in Europe and the classification of soil profiles supplied by EN 1998-1 Code (Eurocode, 2004) did not include volcanic formations until 2010. But (Malheiro, 2007) demonstrated that the shear wave velocities for volcanic deposits allow to characterise these soil types as A (rock, $V_{s,30} > 800$ ms^{-1}) and C (deep deposits of dense or sand, gravel, or stiff clay, 180 ms$^{-1} < V_{s,30} <$ 360 ms^{-1}). So, the main objective here is to enhance a damage estimation for the city of Horta using the method described. The simplified formulation of the EN 1998-1 Code is applied to evaluate the vibration period of the examined masonry buildings (Malheiro, 2007) as:

$$T = \alpha \cdot H^{\beta} \tag{9}$$

where for masonry buildings $\alpha = 0.05$ and $\beta = 0.75$, while H is the maximum height of the building expressed in metres. Table 4 shows the amplification factor, f_{ag}, computed from Eq. (6) for the surveyed typological classes.

Table 4. Amplification factor, f_{ag}, for different soil conditions

Typological Class	H_{mean} [m]	$\boldsymbol{T}$ [s]	f_{ag}				
			A	B	C	D	E
URM-L	3.2	0.12	1.0	1.2	1.0	1.2	1.4
URM-M	6.4	0.20	1.0	1.2	1.2	1.4	1.4
URM-H	9.6	0.27	1.0	1.2	1.2	1.4	1.4

According to these results, the maximum allowable amplification factor for the investigated site ranges from no amplification ($f_{ag} = 1.0$) for soil category A (rock) to 1.4 for soil category E (surface alluvium layer), with a 40% increase in the triggered effects. The amplification factor predicted values are comparable to those proposed in (Giovinazzi, 2009b) for the identical URMs typological classes.

Next, the seismic vulnerability increment (ΔV_I) for each soil category was calculated according to Eq. (8) and the results are presented in Table 5.

Table 5. Vulnerability increments for different soil conditions.

Typological Class	H_{mean} [m]	T [s]	ΔV_I [%]				
			A	B	C	D	E
URM-L	3.2	0.12	0.00	5.00	0.00	4.00	9.00
URM-M	6.4	0.20	0.00	5.00	4.00	8.00	9.00
URM-H	9.6	0.27	0.00	5.00	4.00	8.00	9.00

The expected increase of macroseismic intensity varies from soil class A (with the highest shear wave velocity, $V_{s,30}$) to soil class E (with the lowest $V_{s,30}$), according to the EN 1998-1 classification system. This is due to the correlation between soil type classifications and $V_{s,30}$. The estimated maximum variation in expected macroseismic intensity between these soil classes is 9%. Therefore, the total vulnerability is computed as the combined amount of the vulnerability index, I_v, resulting from the index-based approach (see Section 2.5), and the contributions induced by site effects, ΔV_I, according to the following equation (Chieffo & Formisano, 2019b):

$$\overline{V_I} = I_V + \Delta V_I \tag{10}$$

The updated building vulnerability level is given in Figure 12, including two distinct scenarios for soil classes A and E.

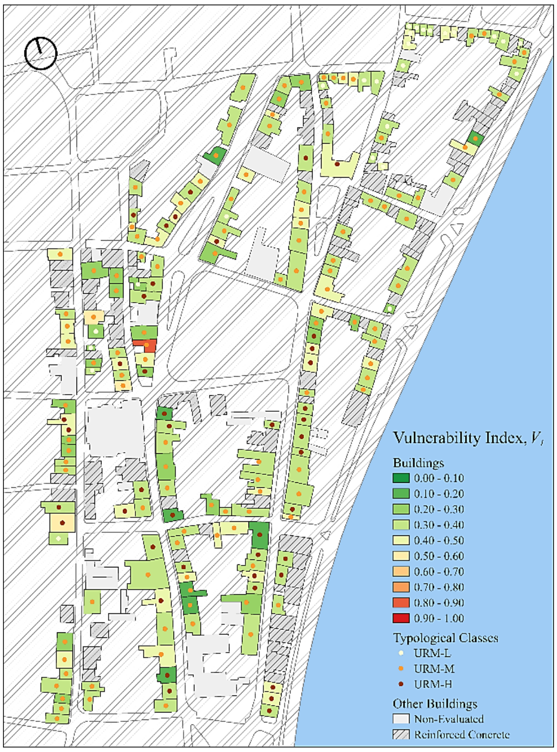

Soil Type A

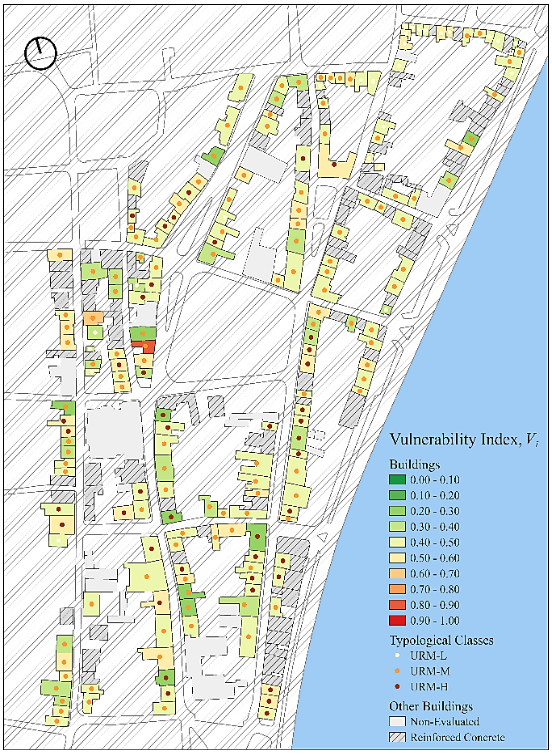

Soil Type E

Figure 12. Global vulnerability maps consider local amplification effects.

4.3. Representation of the site effects in terms of damage curves

In this section, the damage scenarios are correlated to the new global vulnerabilities belonging to the same typological classes, providing a prediction of the expected damage effects. Figure 13 illustrates the mean damage curves calculated by applying Eq. (3) for different soil conditions. According to the obtained outcomes, the worst-case damage scenario is identified with soil category E, which corresponds to a vulnerability index of 0.45 including all typological classes examined. Similarly, as shown in Table 6, the damage generated from the simulated scenario indicates that the damage variation for the URM-L building class is none for soil class C. This is due to the spectral ordinates associated with the elastic response spectrum for soil category C, which is somewhat lower than the response spectrum determined for soil B. It can also be shown that, except for category A (rock), there is an increase in damage ranging from 9.0 % to 17.0 % when including the site effects.

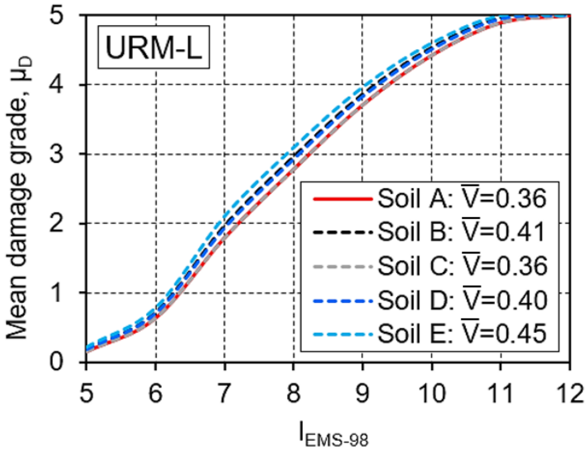

(a)

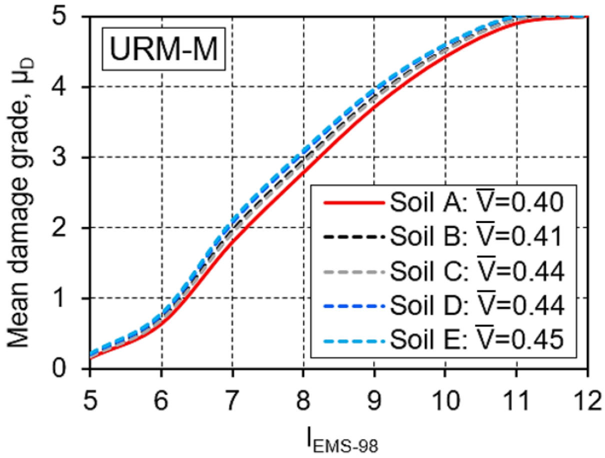

(b)

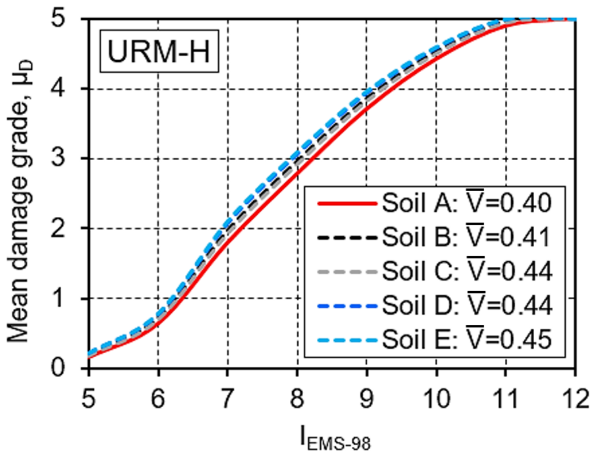

(c)

Figure 13. Damage curves for the examined typologies considering the influence of the geotechnical amplification factor for all soil types.

Table 6. Mean damage increment associated with the different soil types (from A to E).

Typological Class	PGA (ms^{-2})	I_{EMS-98}	$\Delta\mu_D$ [%]				
			Soil type - EC8				
			A	B	C	D	E
URM-L	4.0	VII	-	9.0	-	9.0	17.0
URM-M	4.0	VII	-	9.0	8.0	15.0	17.0
URM-H	4.0	VII	-	9.0	8.0	15.0	17.0

Finally, Figure 14 depicts the damage map, which compares the expected damage for soil class E (worst-case) to the analogous condition obtained by excluding local amplification effects.

(a) With site effects (b) Without site effects

Figure 14. Damage scenarios for soil class E: (a) with and (b) without site effects.

5. Concluding remarks

The ongoing research work presented a streamlined approach for assessing seismic vulnerability despite considering local amplification effects. For this purpose, the historic centre of Horta was chosen for the study to serve as a model. The following are the key outcomes associated with the vulnerability approach that ignores site effects:

- the assessment of the urban sector's building typology was explored to classify structural aggregates based on the structural and typological criteria. The researched urban sector included 313 buildings and the prominent masonry classes were subdivided into three different types based on the number of floors, including URM-L (low stories number), URM-M (medium stories number), and URM-H (high stories number) (high stories number). It was revealed that the URM-L class accounts for roughly 14% of the investigated sample, while the URM-M class accounts for 63% of the reviewed instances, and the URM-H class accounts for 23%.

- the seismic vulnerability was evaluated using an index-based approach, with statistical results indicating a medium to a low physical vulnerability, which corresponds to 59% of the buildings sample with an expected index ranging from 33 to 38;
- by varying the seismic intensity according to the study proposed (Grünthal, 1998), vulnerability curves were defined to describe, on average, the expected damage. It was observed that the expected damage for macroseismic intensity $I_{\text{EMS-98}} < \text{X}$ is primarily D3 (significant damage), whereas, for higher macroseismic intensity ($\text{X} < I_{\text{EMS-98}} < \text{XII}$), the predicted effects resulted in significant damage to the complete collapse of the majority of the building stock in the studied urban region;
- an intensity conversion model based on real accelerograms recorded after the 1998 Azores earthquake has been used to simulate the damage scenario. The main outcomes showed that damage grade D1 damaged all of the studied URM-L buildings (Slight damage). Concerning the URM-M class, the mean damage was assessed to be 0.39, corresponding to 8% of buildings having a damage level of D1. Furthermore, 90% of the investigated buildings suffer damage D2 (Moderate damage) and only 2% of the cases were damaged D3 (Significant damage). Finally, 12% of URM-H buildings had D1 damage and 88% had D2 damage, confirming what happened following the 1998 Azores earthquake.

Next, the site effects were evaluated using a simplified method based on the EN 1998-1 design response spectrum for different soil conditions. Five soil categories were identified due to this particular purpose to assess the impact of the site amplification factor on the structural performance of the investigated urban centre. The major findings indicated that:

- the amplification factor was computed by dividing the maximum acceleration at the bedrock by the corresponding at the foundation for a generic soil type. According to the outcomes, modifying the stratigraphy of the site gave a 40% increase in amplification passing from soil A (rock) to soil E (surface alluvium layer);
- the site effects increased the predicted vulnerability in a range from 5% to 9%, resulting in a maximum damage increase of 17%, in comparison to the case when the site effects were neglected.

Finally, the results revealed that, albeit simplified, the adopted technique provides adequate indications for evaluating the impact of site effects on the expected damage of masonry building compounds, which a step forward regarding seismic scenarios in historic centres. The current study may be enhanced by selecting an appropriate seismogenic source model based on refined physics-ground motion simulation procedures for areas with different structural typologies and lithology settings to develop a further improvement in seismic risk computational methods.

Acknowledgements

This work was partly financed by FCT / MCTES through national funds (PIDDAC) under the R&D Unit Institute for Sustainability and Innovation in Structural Engineering (ISISE), under reference UIDB / 04029/2020, and under the Associate

Laboratory Advanced Production and Intelligent Systems ARISE under reference LA/P/0112/2020.

References

Afak, E. (2001). Local site effects and dynamic soil behavior. *Soil Dynamics and Earthquake Engineering*, *21*(5), 453–458. https://doi.org/10.1016/S0267-7261(01)00021-5.

Atkinson, G. M., & Kaka, S. L. I. (2007). Relationships between felt intensity and instrumental ground motion in the Central United States and California. *Bulletin of the Seismological Society of America*, *97*(2), 497–510. https://doi.org/10.1785/0120060154.

Azizi-Bondarabadi, H., Mendes, N., Lourenço, P. B., & Sadeghi, N. H. (2016). Empirical seismic vulnerability analysis for masonry buildings based on school buildings survey in Iran. *Bulletin of Earthquake Engineering*. https://doi.org/10.1007/s10518-016-9944-1.

Basaglia, A., Aprile, A., Spacone, E., & Pilla, F. (2018). Performance-based Seismic Risk Assessment of Urban Systems. *International Journal of Architectural Heritage*, *12*(7–8), 1131–1149. https://doi.org/10.1080/15583058.2018.1503371.

Bianconi, F., Salachoris, G. P., Clementi, F., & Lenci, S. (2020). A genetic algorithm procedure for the automatic updating of FEM based on ambient vibration tests. Sensors, 20(11), 3315. https://doi.org/10.3390/s20113315.

Biglari, M., D'Amato, M., & Formisano, A. (2021). Rapid seismic vulnerability and risk assessment of Kermanshah historic mosques. *The Open Civil Engineering Journal*, *15*(1).

Biglari, M., & Formisano, A. (2021). *Urban Seismic Risk Analysis Using Empirical Fragility Curves for Kerend-e-Gharb After Mw 7.3, 2017 Iran Earthquake*.

Bindi, D., Cotton, F., & Parolai, S. (2021). Site effects assessment for risk mitigation purposes: Insights from recent European projects. Engineering Geology, 291, 106047. doi: 10.1016/j.enggeo.2021.106047.

Boore, D. M., & Joyner, W. B. (1997). Site amplifications for generic rock sites. *Bulletin of the Seismological Society of America*, *87*(2), 327–341.

Bozorgnia, Y., Hachem, M. M., & Campbell, K. W. (2010). Ground motion prediction equation («Attenuation Relationship») for inelastic response spectra. *Earthquake Spectra*. https://doi.org/10.1193/1.3281182.

Bramerini, F., & Lucantoni, A. (2000). Analysis of different earthquake damage scenarios for emergency planning in Italy. *Management Information Systems*.

Brando, G., Pagliaroli, A., Cocco, G., & Di Buccio, F. (2020). Site effects and damage scenarios: The case study of two historic centers following the 2016 Central Italy earthquake. *Engineering geology*, *272*, 105647.

Brando, G., Rapone, D., Spacone, E., O'Banion, M. S., Olsen, M. J., Barbosa, A. R., Faggella, M., Gigliotti, R., Liberatore, D., Russo, S., Sorrentino, L., Bose, S., & Stravidis, A. (2017). Damage Reconnaissance of Unreinforced Masonry Bearing Wall Buildings After the 2015 Gorkha, Nepal, Earthquake. *Earthquake Spectra*. https://doi.org/10.1193/010817EQS009M.

Calvi, G. M., Pinho, R., Magenes, G., Bommer, J. J., Restrepo-Vélez, L. F., & Crowley, H. (2006). Development of seismic vulnerability assessment methodologies over the past 30 years. *ISET journal of Earthquake Technology*, *43*(3), 75–104.

Clementi, F. (2021). Failure analysis of Apennine masonry churches severely damaged during the 2016 central Italy seismic sequence. Buildings, 11(2), 58. https://doi.org/10.3390/buildings11020058.

Chieffo, N., & Formisano, A. (2019b). The influence of geo-hazard effects on the physical vulnerability assessment of the built heritage: An application in a district of Naples. *Buildings*, *9*(1), 26.

Chieffo, N., & Formisano, A. (2019c). Geo-Hazard-Based Approach for the Estimation of Seismic Vulnerability and Damage Scenarios of the Old City of Senerchia (Avellino, Italy). *Geosciences*, *9*(2), 59. https://doi.org/10.3390/geosciences9020059.

Chieffo, N., & Formisano, A. (2020). Induced Seismic-Site Effects on the Vulnerability Assessment of a Historical Centre in the Molise Region of Italy: Analysis Method and Real Behaviour Calibration Based on 2002 Earthquake. *Geosciences*, *10*(1), 21. https://doi.org/10.3390/geosciences10010021.

Chieffo, N., Formisano, A., & Miguel Ferreira, T. (2019). Damage scenario-based approach and retrofitting strategies for seismic risk mitigation: An application to the historical Centre of Sant'Antimo (Italy). *European Journal of Environmental and Civil Engineering*. https://doi.org/10.1080/19648189.2019.1596164.

Costa, A. (2002). Determination of mechanical properties of traditional masonry walls in dwellings of Faial Island, Azores. *Earthquake Engineering and Structural Dynamics*. https://doi.org/10.1002/eqe.167.

D'Ayala, D. F., Spence R, Oliveira C, & Pomonis A. (1997). Earthquake Loss Estimation for Europe's Historic Town Centres. *Earthquake Spectra*, *13*, 773–793.

Di Ludovico, M., Prota, A., Moroni, C., Manfredi, G., & Dolce, M. (2017). Reconstruction process of damaged residential buildings outside historical centres after the L'Aquila earthquake: Part II—"heavy damage" reconstruction. *Bulletin of Earthquake Engineering*, *15*(2), 693–729.

Dolce, M., Kappos, A., Masi, A., Penelis, G., & Vona, M. (2006). Vulnerability assessment and earthquake damage scenarios of the building stock of Potenza (Southern Italy) using Italian and Greek methodologies. *Engineering Structures*, *28*(3), 357–371. https://doi.org/10.1016/j.engstruct.2005.08.009.

Eurocode, C. (2004). 8: Design of structures for earthquake resistance—Part 1: General rules, seismic actions and rules for buildings (EN 1998-1: 2004). *European Committee for Normalization, Brussels*, *1*(2004).

Ferrante, A., Giordano, E., Clementi, F., Milani, G., & Formisano, A. (2021). FE vs. DE modeling for the nonlinear dynamics of a historic church in central Italy. Geosciences, 11(5), 189. https://doi.org/10.3390/geosciences11050189.

Ferreira, T. M., Maio, R., & Vicente, R. (2017a). Analysis of the impact of large scale seismic retrofitting strategies through the application of a vulnerability-based approach on traditional masonry buildings. *Earthquake Engineering and Engineering Vibration*. https://doi.org/10.1007/s11803-017-0385-x.

Ferreira, T. M., Maio, R., & Vicente, R. (2017b). Seismic vulnerability assessment of the old city centre of Horta, Azores: Calibration and application of a seismic vulnerability index method. *Bulletin of Earthquake Engineering*, *15*(7), 2879–2899.

Ferreira, T. M., Vicente, R., Mendes da Silva, J. A. R., Varum, H., & Costa, A. (2013a). Seismic vulnerability assessment of historical urban centres: Case study of the old city centre in Seixal, Portugal. *Bulletin of Earthquake Engineering*. https://doi.org/10.1007/s10518-013-9447-2.

Ferreira, T. M., Vicente, R., & Varum, H. (2014). Seismic vulnerability assessment of masonry facade walls: Development, application and validation of a new scoring method. *Structural Engineering and Mechanics*. https://doi.org/10.12989/sem.2014.50.4.541.

Giovinazzi, S. (2009b). Geotechnical hazard representation for seismic risk analysis. In *Bulletin of the New Zealand Society for Earthquake Engineering* (Vol. 42, Numero 4, pag. 308). https://doi.org/10.5459/bnzsee.42.3.221-234.

Grünthal, G. (1998). *A. Conseil de l'Europe. European Macroseismic Scale (EMS).*

Kassem, M. M., Nazri, F. M., & Farsangi, E. N. (2020). The seismic vulnerability assessment methodologies: A state-of-the-art review. *Ain Shams Engineering Journal*, *11*(4), 849–864.

Kircher, C. A., Whitman, R. V., & Holmes, W. T. (2006). HAZUS Earthquake Loss Estimation Methods. *Natural Hazards Review*. https://doi.org/10.1061/(ASCE)1527-6988(2006)7:2(45).

Lagomarsino, S., Cattari, S., & Ottonelli, D. (2021). The heuristic vulnerability model: Fragility curves for masonry buildings. *Bulletin of Earthquake Engineering*, *19*(8), 3129–3163.

Lamego, P., Lourenço, P. B., & Sousa, M. L. (2017). Seismic vulnerability and risk analysis of the old building stock at urban scale: Application to a neighbourhood in Lisbon. *Bulletin of Earthquake Engineering*.

Lanzo, G., Silvestri, F., Costanzo, A., d'Onofrio, A., Martelli, L., Pagliaroli, A., Sica, S., & Simonelli, A. (2011). Site response studies and seismic microzoning in the Middle Aterno valley (L'aquila, Central Italy). *Bulletin of Earthquake Engineering*, *9*(5), 1417–1442. https://doi.org/10.1007/s10518-011-9278-y.

Lourenço, P. B., & Roque, J. A. (2006). Simplified indexes for the seismic vulnerability of ancient masonry buildings. *Construction and Building Materials*, *20*(4), 200–208.

Maio, R., Ferreira, T. M., Vicente, R., & Estêvão, J. (2016). Seismic vulnerability assessment of historical urban centres: Case study of the old city centre of Faro, Portugal. *Journal of Risk Research*, *19*(5), 551–580.

Masi, A., Chiauzzi, L., Nicodemo, G., & Manfredi, V. (2020). Correlations between macroseismic intensity estimations and ground motion measures of seismic events. *Bulletin of Earthquake Engineering*, *18*(5), 1899–1932. https://doi.org/10.1007/s10518-019-00782-2.

Milani, G., & Clementi, F. (2018). Advanced seismic assessment of four masonry bell towers in Italy after operational modal analysis (OMA) identification. International Journal of Architectural Heritage, 12(6), 873-882. https://doi.org/10.1080/15583058.2018.1425554.

Mosoarca, M., Onescu, I., Onescu, E., & Anastasiadis, A. (2020). Seismic vulnerability assessment methodology for historic masonry buildings in the near-field areas. *Engineering Failure Analysis*, *115*, 104662. https://doi.org/10.1016/j.engfailanal.2020.104662.

Rapone, D., Brando, G., Spacone, E., & De Matteis, G. (2018). Seismic vulnerability assessment of historic centers: Description of a predictive method and application to the case study of Scanno (Abruzzi, Italy). *International Journal of Architectural Heritage*, *12*(7–8), 1171–1195.

Raptakis, D., Makra, K., Pitilakis, K., & Abrahamson, N. A. (2018). Large scale site effect evaluation and modeling for seismic hazard assessment: The case of Thessaloniki (Greece). Soil Dynamics and Earthquake Engineering, 112, 149-160. doi: 10.1016/j.soildyn.2018.05.013.

Rosti, A., Del Gaudio, C., Rota, M., Ricci, P., Di Ludovico, M., Penna, A., & Verderame, G. M. (2021). Empirical fragility curves for Italian residential RC buildings. *Bulletin of Earthquake Engineering*, *19*(8), 3165–3183. https://doi.org/10.1007/s10518-020-00971-4.

Rota, M., Penna, A., & Strobbia, C. L. (2008). Processing Italian damage data to derive typological fragility curves. *Soil Dynamics and Earthquake Engineering*, *28*(10), 933–947. https://doi.org/10.1016/j.soildyn.2007.10.010.

Salgado-Gálvez, M. A., Zuloaga Romero, D., Velásquez, C. A., Carreño, M. L., Cardona, O.-D., & Barbat, A. H. (2016). Urban seismic risk index for Medellín, Colombia, based on probabilistic loss and casualties estimations. *Natural hazards*, *80*(3), 1995–2021.

Salachoris, G. P., Standoli, G., Betti, M., Pecce, M. R., & Clementi, F. (2023). Evolutionary numerical model for cultural heritage structures via genetic algorithms: a case study in central Italy. Bulletin of Earthquake Engineering, 1-20. https://doi.org/10.1007/s10518-023-01615-z.

Schiavoni, M., Giordano, E., Roscini, F., & Clementi, F. (2023). Numerical assessment of interacting structural units on the seismic damage: a comparative analysis with different modeling approaches. Applied Sciences, 13(2), 972. https://doi.org/10.3390/app13020972.

Spadafora, F., & Alberico, I. (2017). Site effects in Catania city (Sicily, Italy) by 2D synthetic simulations: A large-scale analysis. Journal of Earthquake Engineering, 21(5), 693-712. doi: 10.1080/13632469.2017.1288937.

Toro, G. R., Abrahamson, N. A., & Schneider, J. F. (1997). Model of Strong Ground Motions from Earthquakes in Central and Eastern North America: Best Estimates and Uncertainties. *Seismological Research Letters*, *68*(1), 41–57. https://doi.org/10.1785/gssrl.68.1.41.

Vicente, R., Parodi, S., Lagomarsino, S., Varum, H., & Silva, J. A. R. M. (2011b). Seismic vulnerability and risk assessment: Case study of the historic city centre of Coimbra, Portugal. *Bulletin of Earthquake Engineering*, *9*(4), 1067–1096. https://doi.org/10.1007/s10518-010-9233-3.

Whitman, R. V., Reed, J. W., & Hong, S.-T. (1974). Earthquake Damage Probability Matrices. In *Proceedings of the Fifth World Conference on Earthquake Engineering, Rome, Italy*. https://doi.org/Vol. 2, pp. 2531-2540.

Zonno, G., Musacchio, G., Meroni, F., Oliveira, C. S., Ferreira, M. A., & Neves, F. (2008). *THE 9TH JULY 1998 FAIAL EARTHQUAKE: COMPARISON OF STOCHASTIC FINITE FAULT DAMAGE SIMULATION WITH SURVEYED DATA*.

Zuccaro, G., & Cacace, F. (2015). Seismic vulnerability assessment based on typological characteristics. The first level procedure «SAVE». *Soil Dynamics and Earthquake Engineering*. https://doi.org/10.1016/j.soildyn.2014.11.003.